SCAD:SUPER-CLASS-AWARE DEBIASING FOR LONG-TAILED SEMI-SUPERVISED LEARNING

Anonymous authors
Paper under double-blind review

ABSTRACT

In long-tailed semi-supervised learning (LTSSL), pseudo-labeling often creates a vicious cycle of bias amplification, a problem that recent state-of-the-art methods attempt to mitigate using logit adjustment (LA). However, their adjustment schemes, inherited from LA, remain inherently hierarchy-agnostic, failing to account for the semantic relationships between classes. In this regard, we identify a critical yet overlooked problem of *intra-super-class imbalance*, where a toxic combination of high semantic similarity and severe local imbalance within each super-class hinders effective LTSSL. This problem causes the model to reinforce on its errors, leading to representation overshadowing. To break this cycle, we propose Super-Class-Aware Debiasing (SCAD), a new framework that performs a dynamic, super-class-aware logit adjustment. SCAD leverages the latent semantic structure between classes to focus its corrective power on the most confusable groups, effectively resolving the local imbalances. Our extensive experiments validate that SCAD achieves new state-of-the-art performance, demonstrating the necessity of a super-class-aware approach for robust debiasing.

1 INTRODUCTION

Deep learning models have achieved remarkable success on large, annotated datasets, but creating them is expensive (Deng et al., 2009; Lin et al., 2014). Semi-supervised learning (SSL) is a powerful approach to reduce this cost by using a small labeled dataset with a large unlabeled one (Sohn et al., 2020; Berthelot et al., 2020). However, the performance of SSL is often hindered by the long-tailed distribution of real-world data (Figure 1a), where a few majority classes vastly outnumber many minority classes (Kang et al., 2020; Cui et al., 2019). This imbalance especially creates a vicious cycle in long-tailed semi-supervised learning (LTSSL): a biased model generates biased pseudo-labels, reinforcing the bias and causing performance to drop severely for minority classes (Kim et al., 2020; Wei et al., 2021).

To break this vicious cycle, logit adjustment (LA) (Menon et al., 2021), a powerful method from supervised long-tail learning, has become the *de facto standard* for pseudo-label debiasing in LTSSL. LA applies a static, corrective offset to each class's logits, calculated based on the global class frequencies. The appeal of this approach lies in its theoretical guarantee: LA provides a cost-free, *Fisher-consistent* correction for any given class prior, making it an ideal foundational block for more complex scenarios. Building upon this foundation, recent state-of-the-art methods have made remarkable progress by deriving more sophisticated estimates of the true prior to leverage within the LA framework, such as by estimating the distribution mismatch (Wei & Gan, 2023) or measuring the classifier's intrinsic bias (Lee & Kim, 2024). However, while these methods innovate on how to estimate the global prior, the adjustment scheme itself remains that of LA: a single, uniform correction that is inherently blind to the semantic relationships between classes.

In this paper, we first uncover that this blindness to semantic relationships among classes leads to a critical challenge we term *intra-super-class imbalance*. Specifically, we identify that this problem arises from a toxic combination of two factors, best understood through the example of *truck* and *automobile* on CIFAR10-LT. First, for these classes that have **high semantic similarity**, adjustment mechanisms based on LA offer no solution, as its corrective offset is derived solely from class frequencies and is agnostic to the inter-class similarities that cause model confusion. Second, this challenge is dramatically amplified by the **extreme local imbalance** within their shared *vehicle*

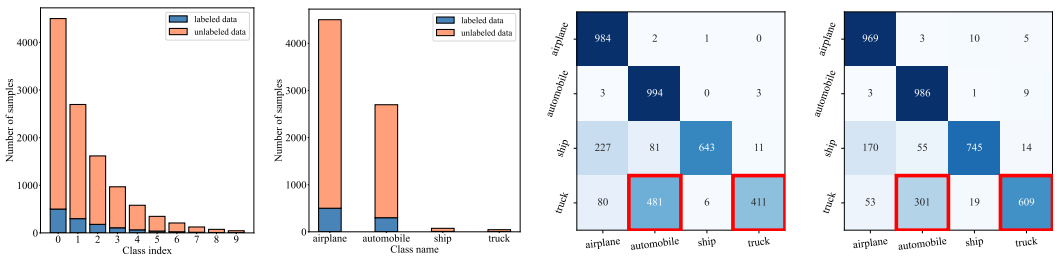

(a) Global Distribution (b) Local Distribution (c) FixMatch + LA (d) FixMatch + SCAD

Figure 1: **Illustration of the *intra-super-class imbalance* problem on CIFAR10-LT.** (a) The overall dataset exhibits a long-tailed distribution. (b) The problem arises from a toxic combination of high semantic similarity and extreme local imbalance, as seen within the *vehicle* super-class. (c) This leads to the failure of LA (Menon et al., 2021), which struggles to distinguish minority classes from their majority neighbors. (d) In contrast, SCAD mitigates these critical misclassifications.

super-class, where *automobile* vastly outnumbers *truck* (Figure 1b). LA's globally derived correction is fundamentally mismatched for this local conflict. Its adjustment for the truck class is determined by its global rarity across the entire dataset, not by the specific, intense competition it faces from *automobile*. This globally calibrated boost is ill-suited to counteract the overwhelming pressure from its direct and dominant competitor. In the context of pseudo-labeling, this dual failure of LA triggers a self-reinforcing loop of bias amplification, leading to representation overshadowing and the systematic misclassification shown in Figure 1c.

To tackle this problem, we propose **S**uper-**C**lass-**A**ware **D**ebiasing **(SCAD)**, a new framework designed to break this cycle by performing a dynamic, super-class-aware logit adjustment. Our approach is driven by a key insight: the debiasing mechanism must be adaptive, dynamically tailoring the corrective force to a sample's predicted semantic group. SCAD implements this by first discovering a latent super-class structure from class names using pre-trained text encoders (e.g., CLIP (Radford et al., 2021)), then training a super-class classifier to infer each unlabeled sample's semantic context, and finally refining standard LA with a super-class-aware correction that uses the super-class posterior as weights for a targeted local correction on top of LA's global adjustment. This allows SCAD to mitigate systematic misclassifications on CIFAR10-LT (Figure 1d), and, as we further show on CIFAR100-LT (Figure 4 and Appendix A.2), to consistently alleviate analogous *intra–super-class* errors on more complex long-tailed benchmarks.

To validate our approach, we conduct experiments on diverse LTSSL benchmarks, ranging from CIFAR10/100-LT (Krizhevsky et al., 2009) to large-scale, fine-grained datasets such as ImageNet-127(Fan et al., 2022) and Food101-LT(Bossard et al., 2014). SCAD proves to be a flexible, pluggable framework that consistently enhances state-of-the-art methods under distribution mismatch.

2 Related Work

Long-tailed Semi-supervised Learning LTSSL addresses the realistic scenario where labeled data is both scarce and imbalanced. Early methods focused on directly manipulating pseudo-labels, for instance, by iterative re-balancing Wei et al. (2021) or refining their distributions Kim et al. (2020); Wang et al. (2022). Subsequently, logit adjustment (LA) Menon et al. (2021) emerged as the *de facto standard* for debiasing, offering a more fundamental solution by directly correcting the model's output logits. The effectiveness and simplicity of LA have made it the foundational block for recent state-of-the-art methods that tackle complex scenarios like distribution mismatch. These advanced methods, such as ACR Wei & Gan (2023) and CDMAD Lee & Kim (2024), innovate by dynamically modulating the strength of the LA correction. ACR achieves this by estimating the mismatch between labeled and unlabeled distributions, while CDMAD does so by measuring the classifier's intrinsic bias. Despite these sophisticated advances, their adjustment schemes remain fundamentally that of LA. Consequently, they are all inherently hierarchy-agnostic and sub-optimal for alleviating the localized confusion between semantic neighbors.

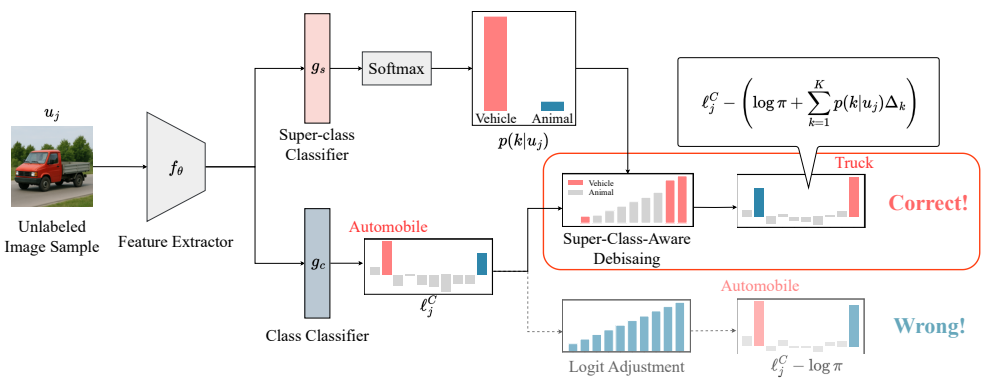

Figure 2: **Illustration of Super-Class-Aware Debiasing (SCAD) mechanism.** For an unlabeled *truck* image, the class classifier initially produces biased logits, incorrectly favoring *automobile*. Standard LA applies a uniform, global correction, which is insufficient to change the outcome. In contrast, our mechanism first uses a reliable super-class classifier to infer the sample's context (*vehicle*). In this context, $p(k|u_j)$, is then used to compute a targeted local adjustment. When this local adjustment is added to the standard LA, it successfully overcomes the initial bias and boosts the logit for the correct class.

Hierarchical and Super-class learning Leveraging class hierarchies to improve recognition is well established. In supervised learning, methods like HD-CNN Yan et al. (2015) and Deep-RTC Wu et al. (2020) use manually defined hierarchies, while SuperDisco Du et al. (2023) discovers super-classes from image features via a graph neural network. However, these approaches are less practical for LTSSL, as they often require pre-defined taxonomies or complex, computationally expensive training. In contrast, SCAD is designed to be lightweight and practical: it constructs super-classes by applying a pre-trained text encoder to class names—without manual hierarchies or pre-trained vision models—and serves as a simple, pluggable debiasing module for existing LTSSL methods.

3 METHOD

We propose Super-Class-Aware Debiasing (SCAD), a multi-stage framework to address *intra–super-class imbalance* in LTSSL. SCAD consists of three components: (i) super-class discovery from semantic information, (ii) a dedicated training procedure for the feature extractor and two classifiers, and (iii) a dynamic logit adjustment mechanism that corrects biased predictions at inference time. We detail each component below, after introducing notation and problem setup.

3.1 PRELIMINARIES

3.1.1 PROBLEM SETUP

Let $\mathcal{D}^l = \{(x_i, y_i)\}_{i=1}^N$ be a labeled dataset and $\mathcal{D}^u = \{u_j\}_{j=1}^M$ an unlabeled dataset, where $x_i, u_j \in \mathbb{R}^d$ denote the d-dimensional inputs. We consider C classes, indexed by $c \in [C] \triangleq \{1, \dots, C\}$. Let N_c be the number of labeled samples in class c and M_c the (generally unknown) number of unlabeled samples in class c. The labeled set is long-tailed with $N_1 \geq N_2 \geq \cdots \geq N_C$ and imbalance ratio $\gamma_l = N_1/N_C$. We similarly define the unlabeled imbalance ratio $\gamma_u = \max_c M_c / \min_c M_c$.

Our model consists of three main components: a feature extractor $f_\theta : \mathbb{R}^d \to \mathbb{R}^p$, a primary class classifier $g_c : \mathbb{R}^p \to \mathbb{R}^C$, and an auxiliary super-class classifier $g_s : \mathbb{R}^p \to \mathbb{R}^K$, where p is the dimensionality of the feature representation and K denotes the number of discovered super-classes. For a given input x, we denote the extracted features as $z = f_\theta(x)$, the class logits as $\ell^c = g_c(z)$, and the super-class logits as $\ell^s = g_s(z)$.

3.1.2 SEMI-SUPERVISED LEARNING.

Our method builds upon the consistency regularization paradigm, as popularized by FixMatch (Sohn et al., 2020). The total loss for the primary SSL is

$$L = L_s + L_u, \tag{1}$$

where L_s is the supervised loss on labeled data and L_u is the unsupervised consistency loss on unlabeled data.

Supervised loss. For a mini-batch $\mathcal{B}_l \subset \mathcal{D}^l$, we apply a weak augmentation $\mathcal{A}_\text{w}$ to x_i and compute

$$L_s = \frac{1}{|\mathcal{B}_l|} \sum_{(x_i,y_i)\in\mathcal{B}_l} \text{CE}\big(\text{softmax}\big(g_c(f_\theta(\mathcal{A}_\text{w}(x_i)))\big),\ y_i\big)\,, \tag{2}$$

where $\text{CE}(\cdot,\cdot)$ denotes the standard cross-entropy with the label y_i treated as a class index.

Unsupervised consistency loss. For a mini-batch $\mathcal{B}_u \subset \mathcal{D}^u$, we obtain a pseudo-label from a weak view and enforce consistency on a strong view. Let $q_j = \text{softmax}\big(g_c(f_\theta(\mathcal{A}_\text{w}(u_j)))\big)$ and $\hat{y}_j = \arg\max_{c\in[C]}(q_j)_c$. We apply a strong augmentation $\mathcal{A}_\text{s}$ to the same sample and compute

$$L_u = \frac{1}{|\mathcal{B}_u|} \sum_{u_j\in\mathcal{B}_u} \mathbb{I}(\max_c(q_j)_c \geq \tau)\ \text{CE}\big(\text{softmax}\big(g_c(f_\theta(\mathcal{A}_\text{s}(u_j)))\big),\ \hat{y}_j\big)\,, \tag{3}$$

where $\tau \in (0,1)$ is a confidence threshold. The mask $\mathbb{I}(\max_c(q_j)_c \geq \tau)$ prevents low-confidence pseudo-labels from contributing to the loss. In practice, $\hat{y}_j$ is treated with stop-gradient.

3.2 SUPER-CLASS GENERATION

The foundation of our method is a structural prior that groups fine-grained classes into meaningful super-classes. We generate this prior automatically from class name semantics, requiring no manual annotation or pre-trained vision models. More details are explained in A.9.

Generation Process. The generation process involves two steps: (1) We convert the names of all C classes into semantic vectors using a pre-trained text encoder (e.g., SBERT (Devlin et al., 2019) or CLIP's text encoder (Radford et al., 2021)). (2) We then apply agglomerative clustering on these vectors. This bottom-up technique builds a dendrogram representing the class hierarchy. By cutting this dendrogram at a level that yields a pre-specified number of clusters (K), we partition the C classes into K super-classes. This process yields a deterministic mapping $\mathcal{M} : \{1,\dots,C\} \to \{1,\dots,K\}$, where $\mathcal{M}(c)$ is the super-class index for class c.

Justification. Our approach of generating super-classes is grounded in the observation that semantic relationships captured by pre-trained text embeddings often correlate with visual taxonomies (Radford et al., 2021). This strategy is particularly advantageous as it sidesteps the need for manual hierarchy creation, which is often infeasible for large-scale or specialized datasets. It is important to clarify that the novelty of our work does not lie in this generation process itself, which is a straightforward application of existing tools. Rather, we employ this process as a simple and effective means to obtain the structural prior required for our main contribution: a new, dynamic debiasing mechanism. Our goal is to show that even an approximate hierarchy can alleviate critical issues when leveraged by a powerful debiasing algorithm.

Crucially, the effectiveness of our framework does not hinge on any single text encoder. This robustness is a key finding, as it proves our method's principle is general and not reliant on a specific, and potentially expensive, text model. SCAD consistently improves performance regardless of the choice of text encoder, from lightweight GloVe (Pennington et al., 2014) to large-scale CLIP. This indicates that SCAD's benefit stems from the debiasing mechanism rather than encoder capacity, a conclusion further supported by our ablations in Section 4.5.

In this work, we obtain super-classes by applying text encoders to class names, but SCAD itself is agnostic to the hierarchy source: it only requires a mapping from classes to super-classes. The same interface can be instantiated using existing taxonomies or manually defined hierarchies. In extremely rare or highly domain-specific settings where class names provide limited semantic signal, ontology- or expert-defined super-classes offer a natural alternative to text-based grouping.

3.3 Training Procedure

The feature extractor f_θ, class classifier g_c, and super-class classifier g_s are trained jointly. The goal of this stage is not only to train the main classifier, but also to train a reliable super-class classifier g_s that can provide a trustworthy signal for our debiasing mechanism.

The rationale for this joint training hinges on the observation that the auxiliary task of super-class classification is inherently simpler and more robust to data imbalance. This robustness stems from two factors: (1) it is a coarse-grained problem with significantly fewer classes ($K \ll C$), and (2) grouping classes often mitigates the label distribution imbalance, as noted in prior work (Du et al., 2023). Consequently, g_s can learn to produce reliable predictions even for minority class samples, providing a stable signal that is crucial for our debiasing mechanism. As we show in Appendix A.4, g_s indeed yields a more balanced and reliable prediction distribution on real-world unlabeled data.

To achieve this, we introduce an auxiliary SSL loss for the super-class task, L_{super}, which mirrors the structure of the primary loss:

$$L_{\text{super}} = L_s^{\text{super}} + L_u^{\text{super}}. \tag{4}$$

Here, the supervised component, L_s^{super}, is the standard cross-entropy loss computed on the labeled batch $\mathcal{B}_l$ using super-class targets $y_i^{\text{super}} = \mathcal{M}(y_i)$, where $\mathcal{M}$ maps each fine-grained class to a super-class (either from a dataset-provided hierarchy or from our automatically discovered grouping). The unsupervised component, L_u^{super}, is a consistency loss computed on the unlabeled batch $\mathcal{B}_u$, enforcing that the model's super-class predictions are consistent across strong and weak augmentations.

The final training objective is a weighted sum of the primary and auxiliary losses:

$$L_{\text{total}} = L + \lambda L_{\text{super}}, \tag{5}$$

where λ is a hyperparameter balancing the two tasks. This objective encourages f_θ to learn representations that are discriminative at both fine-grained and coarse-grained levels.

3.4 Super-Class–Aware Logit Adjustment

This section introduces our framework's core contribution: a novel logit adjustment method, Super-Class–Aware logit Adjustment (SCAD), that addresses a critical limitation of the standard LA. Standard LA applies a static, global correction to the logits based on the class prior distribution π:

$$\ell_j^{\text{LA}} = \ell_j^c - \log \pi, \tag{6}$$

While effective against global class imbalance, this super-class-aware correction is ill-equipped to mitigate local ambiguities, particularly conflicts arising between classes within the same super-class.

SCAD overcomes this limitation with a dynamic, sample-aware adjustment mechanism, illustrated in Figure 2. The process begins by inferring the coarse-grained context for each unlabeled sample u_j. We utilize the super-class classifier, g_s, to obtain a posterior probability distribution over super-classes, $p(k|u_j) = \text{softmax}(\ell_j^s)_k$. This distribution, $p(k|u_j)$, quantifies the estimated likelihood of the sample belonging to each super-class k. For instance, an image of a *truck* would yield a high probability for the *vehicle* super-class, i.e., $p(\text{vehicle}|u_j) \approx 1$.

This inferred context is then used to apply a tailored, super-class-aware adjustment. We pre-calculate an adjustment vector $\Delta_k \in \mathbb{R}^C$ for each super-class k, specifically designed to counteract the *intra-super-class imbalance* within that group. Let $\mathcal{C}_k = \{c \mid \mathcal{M}(c) = k\}$ be the set of all classes belonging to super-class k. The c-th components of Δ_k are defined as:

$$(\Delta_k)_c = \begin{cases} \beta_{k,c}, & \text{if } c \in \mathcal{C}_k, \\ \max_{c' \in \mathcal{C}_k} \beta_{k,c'}, & \text{if } c \notin \mathcal{C}_k, \end{cases} \tag{7}$$

where $\beta_{k,c} = n_{k,c}/(\max_{c' \in \mathcal{C}_k} n_{k,c'})$ is the relative dominance score of class c within its super-class k, based on the sample count or estimated frequency $n_{k,c}$ for class c within super-class k. from a mixture of labeled and high-confidence pseudo-labeled samples: whenever a labeled example with ground-truth label c, or an unlabeled example whose pseudo-label is c with confidence above the FixMatch threshold τ, is assigned to super-class k, we increment $n_{k,c}$ by one. These counts are recomputed periodically (once per epoch in our implementation) using the current classifier. The

Table 1: Results on CIFAR10-LT and CIFAR100-LT datasets for various algorithms and settings.

	CIFAR10-LT				CIFAR100-LT			
	$\gamma = \gamma_l = \gamma_u = 100$		$\gamma = \gamma_l = \gamma_u = 150$		$\gamma = \gamma_l = \gamma_u = 10$		$\gamma = \gamma_l = \gamma_u = 20$	
Algorithm	$N_1 = 500$ $M_1 = 4000$	$N_1 = 1500$ $M_1 = 3000$	$N_1 = 500$ $M_1 = 4000$	$N_1 = 1500$ $M_1 = 3000$	$N_1 = 50$ $M_1 = 400$	$N_1 = 150$ $M_1 = 300$	$N_1 = 50$ $M_1 = 400$	$N_1 = 150$ $M_1 = 300$
Supervised	47.3 ± 0.95	61.9 ± 0.41	44.2 ± 0.33	58.2 ± 0.29	29.6 ± 0.57	46.9 ± 0.22	25.1 ± 1.14	41.2 ± 0.15
w/ LA	53.3 ± 0.44	70.6 ± 0.21	49.5 ± 0.40	67.1 ± 0.78	30.2 ± 0.44	48.7 ± 0.89	26.5 ± 1.31	44.1 ± 0.42
FixMatch	67.8 ± 1.13	77.5 ± 1.32	62.9 ± 0.36	72.4 ± 1.03	45.2 ± 0.55	56.5 ± 0.06	40.0 ± 0.96	50.7 ± 0.25
w/ DARP	74.5 ± 0.78	77.8 ± 0.63	67.2 ± 0.32	73.6 ± 0.73	49.4 ± 0.20	58.1 ± 0.44	43.4 ± 0.87	52.2 ± 0.66
w/ CReST+	76.3 ± 0.86	78.1 ± 0.42	67.5 ± 0.45	73.7 ± 0.34	44.5 ± 0.94	57.4 ± 0.18	40.1 ± 1.28	52.1 ± 0.21
w/ DASO	76.0 ± 0.37	79.1 ± 0.75	70.1 ± 1.81	75.1 ± 0.77	49.8 ± 0.24	59.2 ± 0.35	43.6 ± 0.09	52.9 ± 0.42
w/ DASO + Ours	75.1 ± 0.10	79.2 ± 1.60	69.0 ± 0.61	75.8 ± 0.33	50.0 ± 0.22	58.7 ± 0.28	44.5 ± 0.35	53.2 ± 0.50
FixMatch + LA	75.3 ± 2.45	82.0 ± 0.36	67.0 ± 2.49	78.0 ± 0.91	47.3 ± 0.42	58.6 ± 0.36	41.4 ± 0.93	53.4 ± 0.32
w/ DARP	76.6 ± 0.92	80.8 ± 0.62	68.2 ± 0.94	76.7 ± 1.13	50.5 ± 0.78	59.9 ± 0.32	44.4 ± 0.65	53.8 ± 0.43
w/ CReST+	76.7 ± 1.13	81.1 ± 0.57	70.9 ± 1.18	77.9 ± 0.71	44.0 ± 0.21	57.1 ± 0.55	40.6 ± 0.55	52.3 ± 0.20
w/ DASO	77.9 ± 0.88	82.5 ± 0.08	70.1 ± 1.68	79.0 ± 2.23	50.7 ± 0.51	60.6 ± 0.71	44.1 ± 0.61	55.1 ± 0.72
w/ DASO + Ours	81.6 ± 0.22	84.0 ± 0.99	74.5 ± 1.21	82.2 ± 0.14	51.8 ± 0.28	60.5 ± 0.21	45.7 ± 0.56	55.7 ± 0.57
FixMatch + ACR	81.6 ± 0.19	84.1 ± 0.39	77.0 ± 1.19	80.9 ± 0.22	51.3 ± 0.48	61.1 ± 0.11	44.8 ± 0.21	55.9 ± 0.31
w/ Ours	**83.5** ± 0.16	**85.5** ± 0.03	**78.6** ± 0.56	**83.3** ± 0.20	**52.7** ± 0.11	**61.8** ± 0.21	**45.8** ± 0.20	**56.4** ± 0.10

Table 2: Test accuracy of previous LTSSL algorithms and ours under inconsistent class distributions, i.e., $\gamma_l \neq \gamma_u$, on CIFAR-10-LT and STL10-LT datasets. The γ_l is fixed to 100 for CIFAR-10-LT, while it is set to 10 and 20 for STL10-LT dataset. The best results are in **bold**.

	CIFAR10-LT ($\gamma_l \neq \gamma_u$)				STL10-LT ($\gamma_u = N/A$)			
	$\gamma_u = 1$ (uniform)		$\gamma_u = 1/100$ (reversed)		$\gamma_l = 10$		$\gamma_l = 20$	
Algorithm	$N_1 = 500$ $M_1 = 4000$	$N_1 = 1500$ $M_1 = 3000$	$N_1 = 500$ $M_1 = 4000$	$N_1 = 1500$ $M_1 = 3000$	$N_1 = 150$ $M_1 = 100k$	$N_1 = 450$ $M_1 = 100k$	$N_1 = 150$ $M_1 = 100k$	$N_1 = 450$ $M_1 = 100k$
FixMatch	73.0 ± 3.81	81.5 ± 1.15	62.5 ± 0.94	71.8 ± 1.70	56.1 ± 2.32	72.4 ± 0.71	47.6 ± 4.87	64.0 ± 2.27
w/ DARP	82.5 ± 0.75	84.6 ± 0.34	70.1 ± 0.22	80.0 ± 0.93	66.9 ± 1.66	75.6 ± 0.45	59.9 ± 2.17	72.3 ± 0.60
w/ CReST	83.2 ± 1.67	87.1 ± 0.28	70.7 ± 2.02	80.8 ± 0.39	61.7 ± 2.51	71.6 ± 1.17	57.1 ± 3.67	68.6 ± 0.88
w/ CReST+	82.2 ± 1.53	86.4 ± 0.42	62.9 ± 1.39	72.9 ± 2.00	61.2 ± 1.27	71.5 ± 0.96	56.0 ± 3.19	68.5 ± 1.88
w/ DASO	86.6 ± 0.84	88.8 ± 0.59	71.0 ± 0.95	80.3 ± 0.65	70.0 ± 1.19	78.4 ± 0.80	65.7 ± 1.78	75.3 ± 0.44
FixMatch + ACR	92.1 ± 0.18	**93.5** ± 0.11	85.0 ± 0.09	89.5 ± 0.17	77.1 ± 1.24	83.0 ± 0.32	75.1 ± 0.70	81.5 ± 0.25
w/ Ours	**93.0** ± 0.13	93.4 ± 0.56	**86.1** ± 0.10	**89.8** ± 0.18	**77.8** ± 0.45	**83.6** ± 0.45	**75.8** ± 0.10	**82.0** ± 0.35

normalization in Eq. 7 then yields $\beta_{k,c} \in [0, 1]$, making $(\Delta_k)_c$ a *relative*, rather than absolute, penalty and rendering the dynamic term insensitive to the overall dataset size. Since the SCAD correction term $\sum_k p(k \mid u_j)\, \Delta_k$ is a convex combination of these bounded adjustments, its components are themselves bounded in $[0, 1]$ and thus act as a moderate, local correction on top of the global LA term $-\log \pi$, whose magnitude can be much larger on highly imbalanced datasets. We empirically found this construction fmto be numerically stable across all benchmarks. For the *vehicle* super-class, this formulation assigns a high penalty (up to 1) to the dominant *automobile* class and a smaller penalty to the minority *truck* class. For all classes outside this super-class, a fixed maximum penalty (e.g. set to the strongest suppression level) is applied, preventing potential confusion. This max penalty design is motivated by prior work (Tao et al., 2023)

The final SCAD adjustment is formulated by augmenting the standard LA correction with our sample-aware term. Specifically, we use the inferred super-class posterior $p(k|u_j)$ as a dynamic weight to create a convex combination of the pre-computed adjustment vectors, Δ_k. This yields a single, sample-specific adjustment vector. The complete SCAD formulation is:

$$\ell_j^{\text{SCAD}} \;=\; \ell_j^c - \left(\log \pi + \sum_{k=1}^{K} p(k|u_j) \Delta_k \right), \tag{8}$$

This dynamic formulation is the key to SCAD's effectiveness. As illustrated in Figure 2, for an image of a truck, the model's high confidence in the *vehicle* super-class ($p(\text{vehicle}|u_j) \approx 1$) ensures that final adjustment is dominated by Δ_{vehicle}. This vector applies a large penalty to the competing majority class (*automobile*) and a smaller penalty to the true class (*truck*), resolving the local ambiguity. In stark contrast, standard LA applies a fixed, global correction that is blind to this local context, making it ill-equipped to handle such *intra-super-class* conflicts.

Table 3: Test accuracy on CIFAR100-LT under *uniform* and *reversed* distributions.

Algorithm	CIFAR100-LT ($\gamma_l \neq \gamma_u$)			
	$\gamma_u = 1$ (uniform)		$\gamma_u = 1/10$ (reversed)	
	$N_1 = 50$ $M_1 = 400$	$N_1 = 150$ $M_1 = 300$	$N_1 = 50$ $M_1 = 400$	$N_1 = 150$ $M_1 = 300$
FixMatch	45.5 ± 0.71	58.1 ± 0.72	44.2 ± 0.43	57.3 ± 0.19
w/ DARP	43.5 ± 0.95	55.9 ± 0.32	36.9 ± 0.48	51.8 ± 0.92
w/ CReST	43.5 ± 0.30	59.2 ± 0.25	39.0 ± 1.11	56.4 ± 0.62
w/ CReST+	43.6 ± 1.60	58.7 ± 0.16	39.1 ± 0.77	56.4 ± 0.78
w/ DASO	53.9 ± 0.66	61.8 ± 0.98	$\mathbf{51.0} \pm 0.19$	60.0 ± 0.31
w/ Ours	$\mathbf{54.0} \pm 0.77$	$\mathbf{62.4} \pm 0.98$	48.6 ± 0.19	$\mathbf{60.4} \pm 0.10$
FixMatch + ACR	57.2 ± 0.19	66.7 ± 0.30	51.6 ± 0.12	62.9 ± 0.25
w/ Ours	$\mathbf{59.1} \pm 0.25$	$\mathbf{66.8} \pm 0.22$	$\mathbf{53.4} \pm 0.11$	$\mathbf{63.3} \pm 0.12$

Table 4: Comparison with other LTSSL baselines on CIFAR10/100-LT.

Algorithm	CIFAR-10-LT			CIFAR-100-LT
	$\gamma_l = \gamma_u = 100$	$\gamma_l = 100, \gamma_u = 1$	$\gamma_l = 100, \gamma_u = 1/100$	$\gamma_l = \gamma_u = 20$
FixMatch + SAW	77.5 ± 0.65	$\mathbf{81.2 \pm 0.68}$	72.3 ± 0.65	50.1 ± 0.10
w/ Ours	$\mathbf{79.4 \pm 0.70}$	81.1 ± 0.30	$\mathbf{75.7 \pm 0.57}$	$\mathbf{53.1 \pm 0.16}$
FixMatch + ABC	81.1 ± 1.14	82.7 ± 0.40	68.9 ± 0.61	53.3 ± 0.79
w/ Ours	$\mathbf{82.0 \pm 0.30}$	$\mathbf{83.0 \pm 0.42}$	$\mathbf{73.2 \pm 1.50}$	$\mathbf{55.1 \pm 0.19}$
FixMatch + CoSSL	83.1 ± 0.45	88.8 ± 0.42	$\mathbf{85.1 \pm 0.58}$	53.9 ± 0.78
w/ Ours	$\mathbf{83.3 \pm 0.32}$	$\mathbf{89.0 \pm 0.27}$	84.8 ± 0.47	$\mathbf{55.0 \pm 0.21}$
FixMatch + CDMAD	83.6 ± 0.46	87.5 ± 0.46	77.6 ± 0.70	54.3 ± 0.44
w/ Ours	$\mathbf{85.1 \pm 0.11}$	$\mathbf{87.9 \pm 0.10}$	$\mathbf{79.4 \pm 1.15}$	$\mathbf{54.9 \pm 0.76}$

4 EXPERIMENT

We conducted experiments used datasets in LTSSL, including CIFAR10-LT (Krizhevsky et al., 2009), CIFAR100-LT (Krizhevsky et al., 2009), and STL10-LT (Coates et al., 2011). Additionally, we performed experiments on the ImageNet-127, Food101-LT (Fan et al., 2022) dataset.

Followed by Wei & Gan (2023), we used three different settings: *consistent*, *uniform*, and *reverse*. The *consistent* setting refers to when $\gamma_l = \gamma_u$. The *uniform* setting indicates that $\gamma_u = 1$. Finally, the *reverse* setting describes the case where γ_l and γ_u have reciprocals of the consistent setting.

4.1 IMPLEMENTATION DETAILS

Following DASO (Oh et al., 2022) and ACR (Wei & Gan, 2023) settings, we apply our framework to various existing methods, including FixMatch (Sohn et al., 2020), FixMatch+DASO, and FixMatch+ACR. If the base method does not adopt the LA-based pseudo-label debiasing, we apply only super-class learning.

We conducted the experiment for the LTSSL method in different experiment settings including SAW (Lai et al., 2022), ABC (Lee et al., 2021), CoSSL (Fan et al., 2022), and CDMAD (Lee & Kim, 2024) to show that our framework can enhance the other method in a different setting. For detailed experimental settings, please refer to Appendix A.2. We set the top-1 accuracy as our evaluation metric. All experiments were conducted three times with different random seeds. Please note that the results for ACR differ from those reported in the original paper[1]. this discrepancy arises because the authors mistakenly used a different backbone on CIFAR100-LT.

[1] https://github.com/Gank0078/ACR/issues/5

Table 5: Test accuracy on ImageNet-127. The best results are in **bold**.

Algorithm / ImageNet-127	32×32	64×64
FixMatch	29.7	42.3
w/ DARP	30.5	42.5
w/ DARP+cRT	39.7	51.0
w/ CReST+	32.5	44.7
w/ CReST++LA	40.9	55.9
w/ CoSSL	43.7	53.9
w/ ACR	57.2	63.6
w/ Ours	60.1	66.7
w/ ACR + Ours	**60.5**	**67.0**

4.2 Results on CIFAR10/100-LT and STL10-LT

In case of $\gamma_\ell = \gamma_u$: To demonstrate the effectiveness of our proposed framework, we conducted experiments by additionally incorporating FixMatch + DASO and FixMatch + ACR for comparison. As shown in Table 1, SCAD enhances performance across almost all settings. It shows that SCAD integrates effectively with various existing LTSSL algorithms, yielding a complementary effect. In particular, the CIFAR100-LT performance was impressive with the ACR, where the settings $N_1 = 50$ and $M_1 = 400$ achieved state-of-the-art performance improvements of 2.7% and 2.2% when $\gamma_\ell = \gamma_u = 10$ and $\gamma_\ell = \gamma_u = 20$.

In case of $\gamma_\ell \neq \gamma_u$: In the real world, there can be distributional differences between unlabeled and labeled datasets. Therefore, we conducted experiments with both uniform and reverse settings to explore these scenarios.

We observed overall performance improvements when SCAD was applied to ACR in the uniform and reverse settings. Specifically, as shown in Table 3, SCAD marginally outperformed DASO on CIFAR100-LT in both the uniform and reverse settings. Furthermore, combining ACR with SCAD led to performance gains of up to 2% and 3.4% in the uniform and reverse settings, respectively.

4.3 Results on ImageNet-127 and Food101-LT

On ImageNet-127 (Fan et al., 2022), a challenging 127-class subset of ImageNet with a severe long-tail distribution ($\gamma_u \approx 286$), our method shows a distinct advantage. Following the standard setup with 10% labeled data, our approach outperforms existing baselines, as detailed in Table 5. Notably, it surpasses the strong ACR baseline by a substantial margin of 5.0% at 32×32 resolution and 4.0% at 64×64 resolution. This improvement is particularly noteworthy as ACR represents a highly competitive recent method, highlighting the efficacy of our proposed hierarchical debiasing. Furthermore, when our method is combined with ACR, it achieves new state-of-the-art results, underscoring its high compatibility as a plug-in module. These significant gains, consistent with results on Food101-LT (see Appendix A.6), validate that our approach effectively alleviates the critical problem of *intra-super-class imbalance*—a fine-grained challenge that existing methods have struggled to address.

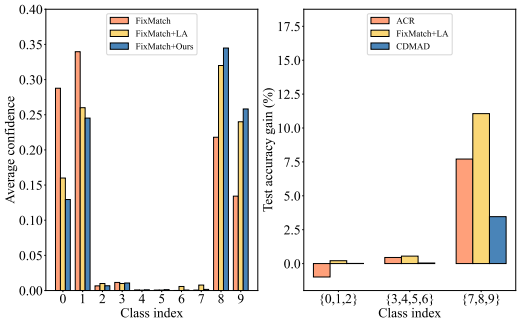

Figure 3: **Left:** figure displays the average confidence scores for minority-class samples (8, 9) of the super-class *vehicle*. Our method effectively reduces confidence in confusing majority classes (0, 1) within the same super-class while increasing confidence in the correct minority classes (8, 9). **Right:** illustration demonstrates that our approach consistently improves accuracy across various LTSSL frameworks, especially benefiting minority classes.

Table 6: Ablation studies of SCAD on CIFAR10-LT and STL10-LT datasets.

Ablations	CIFAR10-LT	STL10-LT
FixMatch	67.8	56.1
+ Super-class learning	69.2	69.0
+ Logit-Adjustment (LA)	76.9	70.4
+ Super-class-Aware Debiasing (SCAD)	**78.7**	**71.3**

Table 7: Comparison of SCAD with ground truth and various text encoders on CIFAR100-LT.

Algorithms	CIFAR100-LT
FixMatch + LA	47.3
w/ Ours with ground truth	50.3
w/ Ours with GloVe	49.7
w/ Ours with SBERT	50.1
w/ Ours with CLIP text encoder	50.4
w/ Ours with text-embedding-ada-002	**50.5**

4.4 Results on other LTSSL Baselines

Table 4 shows that our framework can also be applied effectively to other experiment settings with state-of-the-art methods, we conducted experiments on the three settings of CIFAR10-LT and consistent setting of CIFAR100-LT within the CDMAD (Lee & Kim, 2024), CoSSL (Fan et al., 2022), ABC (Lee et al., 2021) and SAW (Lai et al., 2022) framework. According to CDMAD, when we ran experiments with ACR under CDMAD settings, we observed a performance drop from 84.1 to 81.8 at $N_1 = 1500$ and $M_1 = 3000$. Our framework remains robust when combined with existing LTSSL in different settings. According to Table 4, when combining CDMAD with our framework, which is another state-of-the-art method, there was a 1.6% improvement in the consistent setting, a 0.3% increase in the uniform setting, and a 2.3% improvement in the reverse setting. These results demonstrate that our proposed SCAD framework effectively integrates with diverse LTSSL baselines, further validating its utility and applicability.

4.5 Comprehensive analysis of our method

Ablation study According to Table 6, we evaluated the performance improvements achieved by incrementally adding each component to the algorithms on CIFAR10-LT and STL10-LT under a consistent setting. First, adding the super-class learning component resulted in significant performance gains, with an increase of 2.0% on CIFAR10-LT and 23% on STL10-LT. Finally, adding SCAD yielded additional gains of 9.2% on CIFAR10-LT and 1.1% on STL10-LT. The limited improvement observed from adding SCAD on STL10-LT is likely due to the significant difference in the number of labeled and unlabeled datasets.

Comparison with ground truth super-class labels and various text embedding models As shown in Table 7, there is no performance difference between using our super-class labels generated from text-embeddings-ada-002 (Ryan et al., 2022) or the CLIP text encoder (Radford et al., 2021), and using the ground-truth super-class labels provided in CIFAR100. We further evaluate SCAD on CIFAR100-LT using weaker embeddings such as GloVe (Pennington et al., 2014), SBERT (Nils & Iryna, 2019), and still outperform the baseline. This indicates that our approach remains effective even without large-scale models.

Minority class accuracy comparison As shown in Figure 3, Our method improves the average confidence of minority classes (8,9) over the LA baseline, while correspondingly reducing the confidence of majority classes (0,1) within the same super-class. This result yields consistent gains across diverse LTSSL frameworks, highlighting its general applicability. Moreover, since our approach merely appends a super-class classifier trained in a joint manner, it entails negligible computational overhead (more detailed in Appendix A.7).

Hyperparameter settings we define the confidence threshold τ for class-level predictions as 0.95, following FixMatch. Since super-class learning is expected to converge faster than class-level learning, we set the super-class threshold τ_s to the same value, i.e., $\tau_s = 0.95$, for simplicity and convenience. We determined the number of super-classes K by setting $K = \lceil \frac{C}{4} \rceil$. For a detailed analysis, choosing K and ensuring super-class balance, please refer to Appendix A.4.

5 Conclusion

In this paper, we introduce Super-Class-Aware Debiasing (SCAD), a novel framework designed to tackle the fundamental challenge of *intra-super-class imbalance* in long-tailed semi-supervised learning (LTSSL). Unlike previous approaches that rely solely on global class priors for logit adjustment, SCAD dynamically adapts the corrective force to the semantic context of each sample. To validate the effectiveness of our approach, we conduct extensive experiments on a wide range of LTSSL benchmarks. The results demonstrate that SCAD substantially improves the reliability of pseudo-labels, enhances the learning dynamics of minority classes, and consistently narrows the performance gap caused by long-tailed distributions. Moreover, SCAD achieves state-of-the-art results across diverse datasets, outperforming strong baselines and existing debiasing methods. These findings highlight that incorporating semantic structure and local class relationships into the debiasing process is a powerful strategy, and establish SCAD as a new standard for robust and generalizable learning in real-world imbalanced settings.

6 Limitations and future works

Our study mainly evaluates SCAD within LTSSL. Its effectiveness for other tasks such as detection or segmentation remains an open question and would require further validation. A promising direction for future work is to extend SCAD beyond classification. In particular, applying our idea to more complex tasks such as object detection or semantic segmentation could further demonstrate its utility, as these tasks often suffer from both long-tailed distributions and semantic overlap among categories.

REFERENCES

David Berthelot, Nicholas Carlini, Ekin D Cubuk, Alexey Kurakin, Kihyuk Sohn, Han Zhang, and Colin A Raffel. Remixmatch: Semi-supervised learning with distribution matching and augmentation anchoring. In *International Conference on Learning Representations (ICLR)*, 2020.

Lukas Bossard, Matthieu Guillaumin, and Luc Van Gool. Food-101–mining discriminative components with random forests. In *European conference on computer vision*, pp. 446–461. Springer, 2014.

Adam Coates, Andrew Ng, and Honglak Lee. An analysis of single-layer networks in unsupervised feature learning. in proceedings of the fourteenth international conference on artificial intelligence and statistics. *JMLR Workshop and Conference Proceedings*, 2011.

Ekin D Cubuk, Barret Zoph, Jonathon Shlens, and Quoc V Le. Randaugment: Practical automated data augmentation with a reduced search space. In *Proceedings of the IEEE/CVF conference on computer vision and pattern recognition workshops*, pp. 702–703, 2020.

Yin Cui, Menglin Jia, Tsung-Yi Lin, Yang Song, and Serge Belongie. Class-balanced loss based on effective number of samples. In *Proceedings of the IEEE/CVF Conference on Computer Vision and Pattern Recognition (CVPR)*, pp. 9268–9277, 2019.

Jia Deng, Wei Dong, Richard Socher, Li-Jia Li, Kai Li, and Li Fei-Fei. ImageNet: A large-scale hierarchical image database. In *2009 IEEE Conference on Computer Vision and Pattern Recognition (CVPR)*, pp. 248–255, 2009.

Jacob Devlin, Ming-Wei Chang, Kenton Lee, and Kristina Toutanova. BERT: Pre-training of deep bidirectional transformers for language understanding. In *Proceedings of the 2019 Conference of the North American Chapter of the Association for Computational Linguistics: Human Language Technologies, Volume 1 (Long and Short Papers)*, pp. 4171–4186, 2019.

Terrance DeVries and Graham W Taylor. Improved regularization of convolutional neural networks with cutout. *arXiv preprint arXiv:1708.04552*, 2017.

Yingjun Du, Jiayi Shen, Xiantong Zhen, and Cees G. M. Snoek. Superdisco: Super–class discovery improves visual recognition for the long–tail. In *Proceedings of the IEEE/CVF Conference on Computer Vision and Pattern Recognition (CVPR)*, pp. 19944–19954, 2023.

Yue Fan, Dengxin Dai, Anna Kukleva, and Bernt Schiele. Cossl: Co-learning of representation and classifier for imbalanced semi-supervised learning. In *Proceedings of the IEEE/CVF Conference on Computer Vision and Pattern Recognition (CVPR)*, pp. 14574–14584, 2022.

Kaiming He, Xiangyu Zhang, Shaoqing Ren, and Jian Sun. Deep residual learning for image recognition. *In Proceedings of the IEEE conference on computer vision and pattern recognition*, pp. 770–778, 2016.

Bingyi Kang, Saining Xie, Marcus Rohrbach, Zhicheng Yan, Albert Gordo, Jiashi Feng, and Yannis Kalantidis. Decoupling representation and classifier for long-tailed recognition. In *International Conference on Learning Representations (ICLR)*, 2020.

Jaehyung Kim, Youngbum Hur, Sejun Park, Eunho Yang, Sung Ju Hwang, and Jinwoo Shin. Distribution aligning refinery of pseudo-label for imbalanced semi-supervised learning. In *Advances in Neural Information Processing Systems (NeurIPS)*, pp. 14567–14579, 2020.

Alex Krizhevsky et al. Learning multiple layers of features from tiny images. *arXiv preprint arXiv:0912.1234*, 2009.

Lai, Wang, et al. Smoothed adaptive weighting for imbalanced semi-supervised learning: Improve reliability against unknown distribution data. In *ICML*, 2022. URL `https://api.semanticscholar.org/CorpusID:250341007`.

Hyuck Lee and Heeyoung Kim. Cdmad: Class-distribution-mismatch-aware debiasing for class-imbalanced semi-supervised learning. In *Proceedings of the IEEE/CVF Conference on Computer Vision and Pattern Recognition (CVPR)*, pp. 23891–23900, 2024.

Hyuck Lee, Seungjae Shin, and Heeyoung Kim. Abc: Auxiliary balanced classifier for class-imbalanced semi-supervised learning. In *Advances in Neural Information Processing Systems (NeurIPS)*, pp. 7082–7094, 2021.

Tsung-Yi Lin, Michael Maire, Serge Belongie, James Hays, Pietro Perona, Deva Ramanan, Piotr Dollár, and C. Lawrence Zitnick. Microsoft COCO: Common objects in context. In *European Conference on Computer Vision (ECCV)*, pp. 740–755, 2014.

Aditya Krishna Menon, Sadeep Jayasumana, Ankit Singh Rawat, Himanshu Jain, Andreas Veit, and Sanjiv Kumar. Long-tail learning via logit adjustment. In *International Conference on Learning Representations (ICLR)*, 2021.

Nils and Iryna. Sentence-bert: Sentence embeddings using siamese bert-networks, 2019. URL https://arxiv.org/abs/1908.10084.

Youngtaek Oh, Dong-Jin Kim, and In So Kweon. Daso: Distribution-aware semantics-oriented pseudo-label for imbalanced semi-supervised learning. In *CVPR*, 2022.

Jeffrey Pennington, Richard Socher, and Christopher D Manning. Glove: Global vectors for word representation. In *Proceedings of the 2014 conference on empirical methods in natural language processing (EMNLP)*, pp. 1532–1543, 2014.

Alec Radford, Jong Wook Kim, Chris Hallacy, Aditya Ramesh, Gabriel Goh, Sandhini Agarwal, Girish Sastry, Amanda Askell, Pam Mishkin, Jack Clark, Gretchen Krueger, and Ilya Sutskever. Learning transferable visual models from natural language supervision. In *Proceedings of the International Conference on Machine Learning (ICML)*, 2021.

Ryan, Ted, et al. New and improved embedding model. *OpenAI*, 2022. URL https://openai.com/blog/new-and-improved-embedding-model.

Kihyuk Sohn, David Berthelot, Nicholas Carlini, Zizhao Zhang, Han Zhang, Colin A Raffel, Ekin D Cubuk, Alexey Kurakin, and Chun-Liang Li. Fixmatch: Simplifying semi-supervised learning with consistency and confidence. In *Advances in Neural Information Processing Systems (NeurIPS)*, pp. 596–608, 2020.

Yingfan Tao, Jingna Sun, Hao Yang, Li Chen, Xu Wang, Wenming Yang, Daniel Du, and Min Zheng. Local and global logit adjustments for long-tailed learning. In *Proceedings of the IEEE/CVF international conference on computer vision*, pp. 11783–11792, 2023.

Xudong Wang, Zhirong Wu, Long Lian, and Stella X Yu. Debiased learning from naturally imbalanced pseudo-labels. In *Proceedings of the IEEE/CVF Conference on Computer Vision and Pattern Recognition (CVPR)*, pp. 14647–14657, 2022.

Chen Wei, Kihyuk Sohn, Clayton Mellina, Alan Yuille, and Fan Yang. Crest: A class-rebalancing self-training framework for imbalanced semi-supervised learning. In *Proceedings of the IEEE/CVF Conference on Computer Vision and Pattern Recognition (CVPR)*, pp. 10857–10866, 2021.

Tong Wei and Kai Gan. Towards realistic long-tailed semi-supervised learning: Consistency is all you need. In *Proceedings of the IEEE/CVF Conference on Computer Vision and Pattern Recognition (CVPR)*, pp. 3469–3478, 2023.

Tz-Ying Wu, Pedro Morgado, Pei Wang, Chih-Hui Ho, and Nuno Vasconcelos. Solving long-tailed recognition with deep realistic taxonomic classifier. In *Proceedings of the 16th European Conference on Computer Vision (ECCV)*, volume 12353 of *Lecture Notes in Computer Science*, pp. 171–189. Springer, 2020. doi: 10.1007/978-3-030-58598-3_11.

Zhicheng Yan, Hao Zhang, Robinson Piramuthu, Vignesh Jagadeesh, Dennis DeCoste, Wei Di, and Yizhou Yu. HD–CNN: Hierarchical deep convolutional neural networks for large scale visual recognition. In *Proceedings of the IEEE International Conference on Computer Vision (ICCV)*, pp. 2740–2748. IEEE Computer Society, 2015.

Sergey Zagoruyko and Nikos Komodakis. Wide residual networks. *arXiv preprint arXiv:1605.07146*, 2016.

A Appendix

A.1 The assistance of a Large Language Model (LLM)

This work used a large language model (LLM) solely for language editing (grammar, wording, and minor typographical corrections) during manuscript preparation.

A.2 Experiment setting

For a fair comparison, we integrate our framework with the DASO (Oh et al., 2022), ACR (Wei & Gan, 2023), SAW (Lai et al., 2022), ABC (Lai et al., 2022), CoSSL (Fan et al., 2022), and CDMAD (Lee & Kim, 2024) algorithms using their official code repositories. For example, we use the code for DASO from `https://github.com/ytaek-oh/daso.git`, for ACR from `https://github.com/Gank0078/ACR.git`, and for CDMAD from `https://github.com/LeeHyuck/CDMAD.git`.

When combining FixMatch (Sohn et al., 2020) with our framework, we adopt the ACR settings. It is worth noting that the settings for each algorithm exhibit slight differences. For instance, ACR and CDMAD utilize distinct configurations. The ACR setting is specifically tailored to generate weakly and strongly augmented versions of input images for use within the FixMatch framework.

- **Weak augmentation:** This pipeline applies random horizontal flipping and random cropping with reflective padding to preserve the image structure. These transformations are designed to introduce minimal changes to the input image while maintaining its semantic content.
- **Strong augmentation:** In addition to the weak augmentations, this pipeline uses the RandAugment (Cubuk et al., 2020) method, which applies 2 transformations with 10 magnitude with Cutout (DeVries & Taylor., 2017) operation.

In CDMAD setting, Weak augmentation is same however, there are slight difference in Strong augmentation. CDMAD uses RandAugment with 3 transformations of magnitude 4, followed by the Cutout operation.

The hyperparameter settings differ significantly between ACR and CDMAD. In ACR, the labeled dataset batch size is set to 64, the ratio of the unlabeled batch size to the labeled batch size is set to 1, and the optimizer's learning rate is adjusted using a cosine decay schedule. The learning rate at each step is calculated as $\alpha \cos\left(\frac{7\pi t}{16T}\right)$, where α is the initial learning rate set to 3×10^{-3}, t denotes the current iteration and T is the total number of iterations.

In contrast, CDMAD uses a labeled dataset batch size of 32, the ratio of the unlabeled batch size to the labeled batch size is set to 2, and a learning rate of 2×10^{-3}. All experiments are conducted using one NVIDIA RTX 3090 GPU. The software environment includes PyTorch 2.1.2, TorchVision 0.16.2, and CUDA 12.1.

All settings, We performed the experiments on CIFAR10-LT (Krizhevsky et al., 2009), CIFAR100-LT (Krizhevsky et al., 2009), and STL-10 (Coates et al., 2011) using the WideResNet-28-2 (Zagoruyko & Komodakis, 2016) architecture, and on ImageNet-127 (Fan et al., 2022), Food101-LT(Fan et al., 2022) using the ResNet-50 (He et al., 2016) architecture.

A.3 Intra-superclass-imbalance problem on CIFAR100-LT

We extended our investigation to CIFAR100-LT to prove the prevalence of intra-super-class imbalance. Our results (see Figure 4) show that even on CIFAR-100-LT, substantial imbalance persists within super-classes when using standard methods such as LA: minority classes inside each semantic group remain underserved despite global prior correction. In contrast, SCAD consistently reduces these intra–super-class disparities by explicitly targeting the local bias. These additional findings

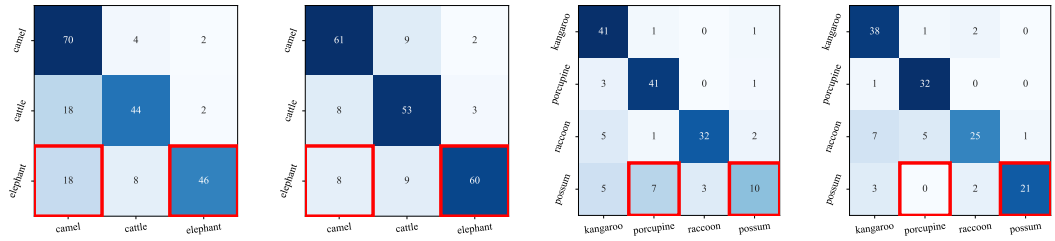

(a) FixMatch + LA (b) FixMatch + Ours (c) FixMatch + LA (d) FixMatch + Ours

Figure 4: Illustration of the *intra-super-class imbalance* problem on CIFAR100-LT. Within the Figure 4a, 4b super-class (e.g., camel and elephant), the model frequently confuses semantically related classes, and SCAD effectively alleviates these errors. A similar pattern appears in the Figure 4c, 4d super-class (e.g., porcupine and possum), where SCAD reduces misclassifications by addressing the local dominance within the group.

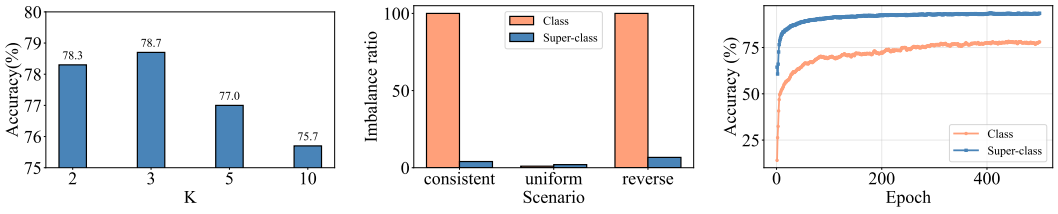

(a) Performance for K (b) Imb-ratio for various settings (c) Performance over epochs

Figure 5: Illustration for balancing super-classes and determining the optimal value of K on CIFAR10-LT

suggest that intra–super-class imbalance is not a CIFAR10-specific artifact and that our solution is robust across different long-tailed datasets.

A.4 Analysis of super-class level distribution

According to Figure 5a, we set $K = \lceil \frac{C}{4} \rceil$. In addition, in Figure 5b we compare the class-level and superclass-level imbalance ratios of unlabeled data under the consistent, uniform, and reverse settings. Note that in the reverse setting, the reciprocal values are not employed. We observe that the imbalance ratio drops sharply in the consistent and reverse settings, while it slightly increases in the uniform setting but still remains nearly identical. Furthermore, owing to this more balanced distribution structure, Figure 5c reports class and super-class level accuracies across training epochs with our method, consistently achieves higher performance at all epochs. These results indicate that the super-class classifier is more balanced and reliable than the class-level counterpart. Experiments on CIFAR100-LT show a similar trend: According to Figure 6a, the performance reaches its maximum around $K = \lceil \frac{C}{4} \rceil$, and when the original unlabeled imbalance ratio γ_u is 10 or lower, the performance difference becomes negligible. (See Figure 6b)

A.5 Visualization on SCAD

To visually demonstrate that our proposed method is particularly beneficial for minority classes, we further compare the confusion matrices of FixMatch, FixMatch + Ours, ACR and ACR+Ours. Specifically, as shown in Figure 7, our method significantly enhances classification performance for minority classes under consistent settings, highlighting the effectiveness of SCAD in alleviating class imbalance.

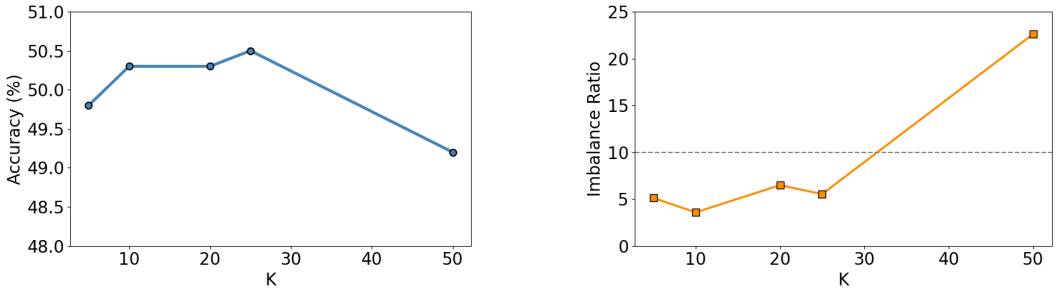

(a) Performance for K (b) Imb-ratio for different K

Figure 6: Illustration for balancing super-classes and determining the optimal value of K on CIFAR100-LT

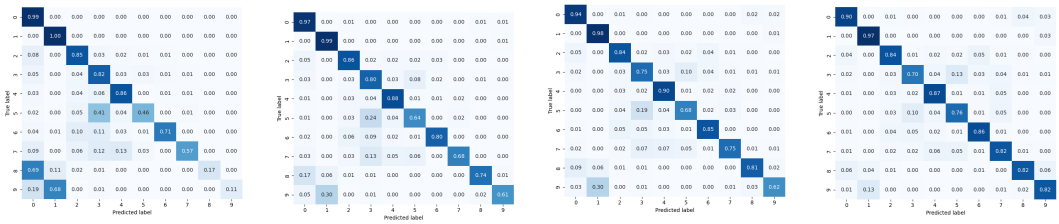

(a) FixMatch (b) FixMatch + Ours (c) ACR (d) ACR + Ours

Figure 7: Confusion matrices of the test set for FixMatch, FixMatch+Ours, ACR, and ACR+Ours under consistent settings.

A.6 FOOD101-LT RESULTS

Food101-LT, we sample 250 labeled and 500 unlabeled images per class, corresponding to imbalance ratios of $\gamma_l = \gamma_u = 50, 100$, followed by CoSSL. According to Table 8, Our method also improves the accuracy on Food101-LT about 3% and 7%, respectively.

Table 8: Test accuracy on Food101-LT with $\gamma_l = \gamma_u = 50, 100$. The best results are in **bold**.

Algorithm	$\gamma = 50$	$\gamma = 100$
FixMatch	42.6	35.3
w/ DARP	42.0	34.2
w/ DARP + cRT	41.5	34.4
w/ CReST+	43.8	31.2
w/ CReST+ + LA	47.7	36.1
w/ CoSSL	49.0	40.4
w/ Ours	**51.0**	**43.5**

A.7 CALIBRATION ANALYSIS ON SCAD

We further evaluate the calibration properties of SCAD compared to FixMatch and LA baselines. We measure calibration using Expected Calibration Error (ECE), which quantifies the discrepancy between predicted confidence and empirical accuracy.FixMatch exhibits severe miscalibration in tail classes, with ECE values reaching up to 0.59, while SCAD reduces these errors substantially. This indicates that SCAD alleviates underconfidence in tail classes and achieves a more balanced calibration across head and tail. We futher evaluated calibration by integrating SCAD into ACR and observed consistent improvements across all frequency groups. The ECE drops from 0.1018 to 0.0517 (Head), 0.1339 to 0.1228 (Medium), and from 0.1654 to 0.0926 (Tail). These results show

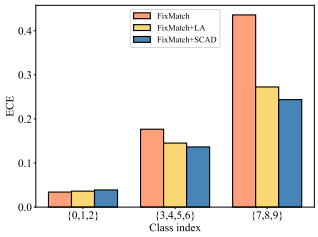

Figure 8: ECE analysis on CIFAR10-LT

Table 9: ECE comparison between ACR and ACR+Ours

Method	Head	Medium	Tail
ACR	0.1018	0.1339	0.1654
ACR+Ours	**0.0517**	**0.1228**	**0.0926**

that SCAD not only preserves performance but also substantially enhances prediction reliability, especially for tail classes.

A.8 Training time analysis

As presented in Table 10, the reported time represents the training time per epoch. The difference between our method and the baseline is approximately 1 second, which is negligible in practice.

A.9 Detailed information about the super-class

We retrieved descriptions for each class name using the Wikipedia API, and for convenience, we only used the first sentence of the returned summary. If no corresponding Wikipedia entry exists, we simply use the class name itself. Agglomerative clustering is performed using the clustering module from scikit-learn. As previously mentioned, we set $K = \lceil \frac{C}{4} \rceil$. Specifically, for CIFAR10-LT (Krizhevsky et al., 2009) and STL10-LT (Coates et al., 2011), $K = 3$, for CIFAR100-LT (Krizhevsky et al., 2009), $K = 25$ and for ImageNet-127 (Fan et al., 2022), $K = 32$. The groupings for CIFAR10-LT, STL10-LT, CIFAR100-LT and ImageNet-127 are detailed in Table 11 and Table 13. These groupings are determined using the text-embedding-ada-002 model (Ryan et al., 2022).

Table 10: Training time comparison (seconds) per epoch

Method	FixMatch	FixMatch+Ours	ACR	ACR+Ours
Time (s)	28	29	35	36

Table 11: Super-class table on CIFAR10-LT. We use the Wikipedia API to retrieve a summary for a given query and perform agglomerative clustering using the text-embedding-ada-002 model, setting the number of clusters to 3.

Cluster	**Classes**
Cluster 0	0: airplane, 1: automobile, 8: ship, 9: truck
Cluster 1	2: bird, 6: frog
Cluster 2	3: cat, 4: deer, 5: dog, 7: horse

Table 12: Super-class table on CIFAR100-LT. We use the Wikipedia API to retrieve a summary for a given query and perform agglomerative clustering using the text-embedding-ada-002 model, setting the number of clusters to 25.

Cluster	**Classes**
Cluster 0	1: aquarium_fish, 26: crab, 45: lobster, 77: snail, 99: worm
Cluster 1	27: crocodile, 29: dinosaur, 44: lizard, 73: shark, 78: snake, 93: turtle
Cluster 2	21: chimpanzee, 42: leopard, 43: lion, 88: tiger
Cluster 3	54: orchid, 62: poppy, 70: rose, 82: sunflower, 92: tulip
Cluster 4	58: pickup_truck, 69: rocket, 85: tank, 89: tractor
Cluster 5	2: baby, 11: boy, 35: girl, 46: man, 98: woman
Cluster 6	22: clock, 86: telephone, 87: television
Cluster 7	6: bee, 7: beetle, 14: butterfly, 18: caterpillar, 24: cockroach, 79: spider
Cluster 8	36: hamster, 50: mouse, 65: rabbit, 74: shrew, 75: skunk, 80: squirrel
Cluster 9	0: apple, 51: mushroom, 53: orange, 57: pear, 83: sweet_pepper
Cluster 10	5: bed, 20: chair, 25: couch, 94: wardrobe
Cluster 11	23: cloud, 71: sea
Cluster 12	33: forest, 49: mountain, 60: plain
Cluster 13	9: bottle, 10: bowl, 28: cup
Cluster 14	13: bus, 81: streetcar, 90: train
Cluster 15	15: camel, 19: cattle, 31: elephant
Cluster 16	17: castle, 37: house, 76: skyscraper
Cluster 17	16: can, 39: keyboard, 40: lamp, 61: plate, 84: table
Cluster 18	32: flatfish, 67: ray, 91: trout
Cluster 19	30: dolphin, 95: whale, 72: seal
Cluster 20	8: bicycle, 41: lawn_mower, 48: motorcycle
Cluster 21	3: bear, 4: beaver, 34: fox, 55: otter, 97: wolf
Cluster 22	12: bridge, 68: road
Cluster 23	38: kangaroo, 63: porcupine, 66: raccoon, 64: possum
Cluster 24	47: maple_tree, 52: oak_tree, 56: palm_tree, 59: pine_tree, 96: willow_tree

Table 13: Super-class table on ImageNet-127. We use the Wikipedia API to retrieve a summary for a given query and perform agglomerative clustering using the text-embedding-ada-002 model, setting the number of clusters to 32.

Cluster	Classes
Cluster 0	17: electronic_equipment, 43: light, 60: camera, 99: magazine, 125: monitor
Cluster 1	16: furniture, 58: litter, 118: cushion
Cluster 2	2: jewelry, 22: hairpiece, 36: protective_garment, 44: garment, 45: nightwear, 50: uniform, 55: glove, 84: hosiery, 90: gown, 113: dress
Cluster 3	27: pot, 28: dish, 30: rod, 42: home_appliance, 71: toiletry, 80: pan, 94: cleaning_implement, 106: cooker, 109: turner
Cluster 4	29: athlete, 34: game_equipment, 41: golf_equipment, 47: gymnastic_apparatus, 53: sports_implement, 110: participant, 115: diver
Cluster 5	31: frozen_dessert, 37: sauce, 39: dip, 63: pudding, 74: entree, 77: cracker, 111: concoction
Cluster 6	9: platform, 32: weight, 59: system, 76: structure, 105: sign, 121: drill_rig
Cluster 7	19: plaything
Cluster 8	75: ceratopsian, 86: mammal, 104: bird
Cluster 9	25: bus, 46: fare, 56: sled, 98: passenger_train
Cluster 10	38: ray, 79: plectognath, 107: shark, 108: ganoid, 124: food_fish, 126: soft_finned_fish
Cluster 11	72: wine, 81: punch, 114: coffee
Cluster 12	8: globule, 21: stick, 66: tissue, 83: covering
Cluster 13	11: fungus, 14: coelenterate, 54: echinoderm, 65: arthropod, 68: mollusk
Cluster 14	88: rescue_equipment, 91: safety_belt
Cluster 15	52: spacecraft, 64: rocket, 67: heavier_than_air_craft, 112: lighter_than_air_craft
Cluster 16	18: sailing_vessel, 35: ship, 93: oar, 119: boat
Cluster 17	6: anguid_lizard, 24: teiid_lizard, 49: lacertid_lizard, 78: gecko, 87: agamid, 102: venomous_lizard, 116: iguanid, 122: chameleon
Cluster 18	20: board, 120: bar
Cluster 19	95: bath_linen, 103: fabric
Cluster 20	1: vegetable, 4: fruit, 40: fodder, 51: flower
Cluster 21	70: pen, 101: eraser
Cluster 22	3: ligament
Cluster 23	13: frog, 89: snake, 96: turtle, 97: salamander, 100: worm
Cluster 24	69: cistern, 117: container
Cluster 25	0: loaf_of_bread, 73: bun
Cluster 26	5: cap, 26: helmet, 123: hat
Cluster 27	15: alligator, 62: crocodile
Cluster 28	12: device, 23: tool, 48: sharpener, 57: kit, 85: key, 92: duplicator
Cluster 29	10: military_vehicle
Cluster 30	33: geological_formation
Cluster 31	7: damselfish, 61: butterfly_fish, 82: scorpaenid